PATIENTS AND METHODS

Subjects

Between December 2001 and March 2005, 205 patients with peripheral lung cancer more than 1 cm in size prospectively underwent FDG-PET and CT scanning during the month before surgery. A total of 2057 lymph node stations in these 205 patients were evaluated. The histological type of lung cancer was adenocarcinoma in 151 patients, squamous cell carcinoma in 37, large cell carcinoma in eight, small cell carcinoma in two, adenosquamous carcinoma in four, carcinosarcoma in two and atypical carcinoid in one (Table 1). The histological criteria were based on the 1999 World Health Organization classification (8). The pathological N stages were N0 in 143, N1 in 31, N2 in 24 and N3 in seven. The classification of lymph nodes was done according to the original lymph node map of lung cancer (9). All patients underwent pneumonectomy, lobectomy, or segmentectomy with mediastinal lymph node dissection, except for seven patients with clinical N3 disease in whom pathological N-stages were evaluated by mediastinoscopy and/or scalene node biopsy.

FDG-PET Scanning

Patients were instructed to fast for at least 4 h prior to intravenous (IV) administration of ^{18}F-FDG. The administered dosage of ^{18}F-FDG was 125 μCi/kg (4.6 MBq/kg) for non-diabetic patients and 150 μCi/kg (5.6 MBq/kg) for diabetic patients. PET imaging was performed approximately 60 min after administration of the FDG with a POSICAM.HZL m-POWER (Positron Co., Houston, Texas, USA). Initially no attenuation-corrected emission scans were obtained during the two-dimensional, high-sensitivity mode for 4 min per bed position, taken from the vertical-skull through the mid-thighs. Immediately thereafter, a two-bed-position attenuation-corrected examination was performed with 6 min for the emission sequence and 6 min for the transmission sequence at each bed position. The images were usually reconstructed in a 256 × 256 matrix by using ordered subset expectation maximization corresponding to a pixel size of 4 × 4 mm, with section spacing of 2.66 mm.

Table 1. Characteristics of patients

Variable	Data
Age (years)	67 ± 19
Sex	
Male	134
Female	71
Tumor size (cm)	3.0 ± 1.8
Histology	
Adenocarcinoma	151
Squamous cell carcinoma	37
Large cell carcinoma	8
Small cell carcinoma	2
Adenosquamous carcinoma	4
Carcinosarcoma	2
Atypical carcinoid	1
Pathological N stage	
N0	143
N1	31
N2	24
N3	7
Total	205

N Staging by PET Scanning

PET data were evaluated visually and/or semi-quantitatively. Based on visual findings, the lymph nodes showing clearly greater or less FDG-uptake than the mediastinal blood pool were diagnosed as positive and negative, respectively. Two examiners (A.E. and K.U.), who were blinded for the pathological N-stage, evaluated the visual findings of PET. For the lymph nodes showing similar FDG-uptake to the mediastinal blood pool or where there was disagreement between the two examiners, semi-quantitative analysis was used as reported previously (10). Briefly, the regions of interest (ROIs) were placed in the lymph nodes and cerebellum. The highest activities in both the lymph node ROI (L) and the cerebellum ROI (C) were measured. The contrast ratio (CR) was calculated by L/C in each lymph node as an index of FDG uptake. The cut-off value was determined as 0.25, i.e. lymph nodes with CR $\geq$ 0.25 were defined as positive and those with CR $<$ 0.25 as negative.

N Staging by CT Scanning

Spiral CT was performed using a ProSeed SA (General Electric Medical System, Milwaukee, USA). The following acquisition parameters were used: high voltage (120 kV), tube load 160 mA, window level −500 Hounsfield units (HU) and window width 1500 HU. The entire thorax was scanned with 0.5 or 1-cm thick sections at 1 breath hold with maximum inspiration. The criterion of CT definition for suspected metastasis of the lymph node was a short-axis diameter of 1.0 cm or larger. Enhanced CT was additionally conducted for patients with CT-negative and PET-positive lymph nodes. The same two examiners for N-staging by PET evaluated the CT findings. For lymph nodes showing disagreement between the two examiners, N-sages were determined after their discussion.

Statistical Analysis

True-positive (TP), true-negative (TN), false-positive (FP) and false-negative (FN) results of PET and CT scanning for lymph node metastasis were compared with the results of pathological diagnosis. Sensitivity was calculated as TP/TP + FN, specificity as TN/TN + FP, positive predictive

value as TP/TP + FP, negative predictive value as TN/TN + FN and accuracy as TP + TN/Total. The advantages of PET over CT were evaluated for each pathological N-stage, lymph node location and each histological type. All data were analyzed for significance by using the Stat View software χ^2 test. Differences at $P < 0.05$ were accepted as significant. All values in the text and tables are given as mean ± SD.

RESULTS

Table 2 shows the correlation between the N-staging by PET and CT and pathological N-stage. PET was able to diagnose N0, N2 and N3 diseases more accurately than CT with significant difference ($P = 0.03$, 0.01 and 0.02, respectively). However, there was no difference between PET and CT in the accuracy in diagnosing N1 disease ($P = 0.4$).

Of the 2057 lymph node stations examined, 15 showed similar FDG-uptake to the mediastinal blood pool. Of those 15 lymph nodes, six showed CR ≥ 0.25 (positive) and the remaining nine showed CR < 0.25 (negative). PET scanning yielded TP in 85 lymph node stations, FN in 46, FP in 11 and TN in 1915 (Table 3). For the same lymph node stations, CT scanning yielded TP in 49 lymph node stations, FN in 82, FP in 22 and TN in 1904. As a result, the sensitivity of PET was 0.65, which was significantly higher than 0.37 of CT ($P < 0.0001$). The positive predictive value of PET was 0.89, which was significantly higher than 0.7 of CT ($P = 0.02$). However, there was no significant difference in specificity, accuracy and negative predictive value between the two diagnostic modalities.

The locations of FP lymph node stations revealed by PET and CT are shown in Table 4. Of the 670 upper mediastinal lymph node stations without metastasis, PET showed FP less frequently than CT ($P = 0.001$). One FP upper mediastinal lymph node, demonstrated by PET was Botallo's lymph node, showed lymphadenitis probably as a result of tuberculosis accompanying the adenocarcinoma. The other locations of FP lymph nodes did not show any difference between PET and CT.

Table 2. Coincidence of N-staging by PET and CT with pathological N-stage

Pathological N-stage	No. of coincidences with pathological N-stage		Difference
	PET	CT	
N0 ($n = 143$)	138	129	$P = 0.03$
N1 ($n = 31$)	19	16	NS
N2 ($n = 24$)	16	7	$P = 0.01$
N3 ($n = 7$)	7	3	$P = 0.02$

PET, positron emission tomography; CT, computed tomography; NS, not significant.

The locations of FN lymph node stations revealed by PET and CT are shown in Table 5. For the upper mediastinal, lower mediastinal and supra-clavicle lymph nodes with metastasis, PET showed FN less frequently than CT ($P = 0.001$, 0.04 and 0.003). However, for hilar lymph nodes, there was no significant difference of FN between PET and CT.

The difference of histological types in patients who were understaged or overstaged by PET and CT are shown in Tables 6 and 7. For adenocarcinoma, PET showed significantly less understaging than CT ($P = 0.02$) (Table 6). For squamous cell carcinoma, PET showed significantly less overstaging than CT (Table 7) ($P = 0.005$). All seven squamous cell carcinoma patients who were overstaged by CT were heavy smokers, whose Brinkman Index was 680–2400 (mean ± SD: 1444 ± 525).

DISCUSSION

Several criteria have been used to detect lymph node metastases of lung cancer using PET scanning, including accumulation of FDG without objective criteria (6, 11),

Table 3. PET and CT analyses with pathological diagnosis

Diagnosis	No. of lymph node stations		Total
	With metastasis	Without metastasis	
PET			
Positive	85	11	96
Negative	45	1915	1961
CT			
Positive	49	22	71
Negative	82	1904	1986
Total	131	1926	2057

PET, positron emission tomography; CT, computed tomography.

Table 4. False positive lymph node stations with PET and CT

Locations of LNS	No. of LNS without metastasis	False positive with		Difference
		PET	CT	
Upper mediastinum	670	1	12	$P = 0.001$
Lower mediastinum	510	4	3	NS
Hilar	745	4	7	NS
SCN	1	1	0	NS
Total	1926	10	22	

PET, positron emission tomography; CT, computed tomography; LNS, lymph node station; SCN, supra clavicle lymph node; NS, not significant.

Table 5. False negative lymph node stations with PET and CT

Locations of LNS	No. of LNS without metastasis	False positive with		Difference
		PET	CT	
Upper mediastinum	47	14	30	$P = 0.001$
Lower mediastinum	8	2	6	$P = 0.04$
Hilar	70	30	40	$P = 0.1$
SCN	6	1	6	$P = 0.003$
Total	128	45	82	

PET, positron emission tomography; CT, computed tomography; LNS, lymph node station; SCN, supra clavicle lymph node.

Table 6. Difference of histological types whose N-stages were understaged by PET and CT

Histological type	No. of patients	Understaging by	
		PET	CT
Adenocarcinomas	151	11	24*
Non-adenocarcinomas	54	8	13
Total	205	19	37

PET, positron emission tomography; CT, computed tomography.
*Adenocarcinomas are more frequently understaged by CT than by PET ($I = 0.02$).

accumulation greater than mediastinal blood flow (2–4), and CR with the paravertebral muscles (12). We evaluated the lymph nodes with similar FDG-uptake to mediastinal blood pool by using the activity ratio in comparison to the cerebellum, as reported previously (10), because accumulation of FDG in the cerebellum was more stable than that in mediastinal blood flow or muscle.

While several authors have reported the superiority of PET over CT for N-staging of lung cancer (1–7), the present study showed that PET was able to identify N0, N2 and N3 diseases significantly more accurately than CT. However, there was no difference between the two modalities for N1 disease. These results appeared to be supported by data obtained by Vesselle et al., who reported that PET scanning could not reliably identify N1 disease, with only 6 of 21 cases identified (13).

It is well known that the inflammatory condition of lymph nodes can cause FP results of FDG-PET in lung cancer. Takamochi et al. reported that 10 of 71 patients (14%) with NSCLC showed FP lymph nodes with PET (14). While they did not show the location of the FP lymph nodes, the present study demonstrated that PET showed a lower frequency of FP in the upper mediastinal lymph nodes than CT. Thus we concluded that PET-positive lymph nodes in the upper

Table 7. Difference of histological types whose N-stages were overstaged with PET and CT

Histological type	No. of patients	Overstaging by	
		PET	CT
Squamous cell carcinomas	37	0	7*
Non-squamous cell carcinomas	168	5	12
Total	205	5	19

PET, positron emission tomography; CT, computed tomography.
*Squamous cell carcinomas are more frequently overstaged by CT than by PET ($P = 0.005$).

mediastinum could be truly positive for metastasis, making it possible to reduce the need of mediastinoscopy in such patients. However, because there was some possibility of FP in the lower mediastinum and hilar nodes, transbronchial needle or thoracoscopic biopsy is recommended for these regions.

In the analysis of histological types, the present study showed that PET was able to reduce the incidences of FN in adenocarcinoma and FP in squamous cell carcinoma in comparison with CT. Ohta et al. reported that nodal micrometastasis was detected by immunohistochemistry in 20% of patients with adenocarcinoma 1–2 cm in size, whereas it was not found in any patients with squamous cell carcinoma of the same size (15). Mori et al. reported that lymph node metastases from adenocarcinoma frequently showed normal size, resulting in lower sensitivity of N-staging by CT than those from squamous cell carcinoma (16). They also reported that CT scanning showed FP lymph nodes more frequently in squamous cell carcinoma than in adenocarcinoma (16). Because the present study examined peripheral-type lung cancer, there were no enlarged lymph nodes caused by inflammation, such as obstructive pneumonia and atelectasis. Because all seven patients with squamous cell carcinoma whose N-stages were overstaged by CT smoked heavily, the enlarged lymph nodes could be caused by smoking.

We conclude that PET is more advantageous for lymph node staging than CT. However, the advantage depends on the lymph node locations and histological types. Realizing the characteristic advantages of PET is useful for accurate lymph node staging in lung cancer.

References

1. Dwamena BA, Sonnad SS, Angobaldo JO, Wahl RL. Metastases from non-small cell lung cancer: mediastinal staging in the 1990s – meta-analytic comparison of PET and CT. *Radiology* 1999;213:530–6.
2. Gupta NC, Tamin WJ, Graeber GG, Bishop HA, Hobbs GR. Mediastinal lymph node sampling following positron emission tomography with fluorodeoxyglucose imaging in lung cancer staging. *Chest* 2001;120:521–7.
3. Gupta NC, Graeber GM, Bishop HA. Comparative efficacy of positron emission tomography with fluorodeoxyglucose in evaluation of small (<1 cm), intermediate (1 to 3 cm), and large (>3 cm) lymph node lesions. *Chest* 2000;117:773–8.

4. Graeter TP, Hellwig D, Hoffman K, Ukena D, Kirsch CM, Schafers HJ. Mediastinal lymph node staging in suspected lung cancer: comparison of positron emission tomography with F-18-fluorodeoxyglucose and mediastinoscopy. *Ann Thorac Surg* 2003;75:231–6.
5. Chin R Jr, Ward R, Keyes JW, Choplin RH, Reed JC, Wallenhaupt S, et al. Mediastinal staging of non-small cell lung cancer with positron emission tomography. *Am J Respir Crit Care Med* 1995;152:2090–6.
6. Bury T, Paulus P, Dowlati A, Corhay JL, Weber T, Ghaye B, et al. Staging of the mediastinum: value of positron emission tomography imaging in non-small cell lung cancer. *Eur Respir J* 1996;9:2560–4.
7. Valk PE, Pounds TR, Hopkins DM, Haseman MK, Hofer GA, Greiss HB, et al. Staging non-small cell lung cancer by whole-body positron emission tomography imaging. *Ann Thorac Surg* 1995;60:1573–82.
8. Travis WE, Colby TV, Corrin B, Shimosato Y, Brambilla E. World Health Organization international histological classification of tumours. Histological typing of lung and pleural tumours. 3rd edn. (In collaboration with LH Sobin and pathologists from 14 countries). Berlin: Springer; 1999.
9. Naruke T, Suemasu K, Ishikawa S. Lymph node mapping and curability at various levels of metastasis in resected lung cancer. *J Thorac Cardiovasc Surg* 1978:832–9.
10. Nomori H, Watanabe K, Ohtsuka T, Naruke T, Suemasu K, Uno K. The size of metastatic foci and lymph nodes yielding false-negative and false-positive lymph node staging with positron emission tomography in patients with lung cancer. *J Thorac Cardiovasc Surg* 2004;127:1087–92.
11. Lowe VJ, Fletcher JW, Gobar L, Lawson M, Kirchner P, Valk P, et al. Prospective investigation of positron emission tomography in lung nodules. *J Clin Oncol* 1998;16:1075–84.
12. Yasukawa T, Yoshikawa K, Aoyagi H, Yamamoto N, Tamura K, Suzuki K, et al. Usefulness of PET with ^{11}C-Methionine for the detection of hilar and mediastinal lymph node metastasis in lung cancer. *J Nucl Med* 2000;41:283–90.
13. Vesselle H, Pugsley JM, Vallieres E, Wood DE. The impact of fluorodeoxyglucose F 18 positron-emission tomography on the surgical staging of non-small cell lung cancer. *J Thorac Cardiovasc Surg* 2002;124:511–9.
14. Takamochi K, Yoshida J, Murakami K, Niho S, Ishii G, Nishimura M, et al. Pitfalls in lymph node staging with positron emission tomography in non-small cell lung cancer patients. *Lung Cancer* 2005;47:235–42.
15. Ohta Y, Oda M, Wu J, Tsunezuka Y, Hiroshi M, Nomura A, et al. Can tumor size be guide for limited surgical intervention in patients with peripheral non-small cell lung cancer? *J Thorac Cardiovasc Surg* 2001;122:900–6.
16. Mori K, Yokoi K, Saito Y, Tominaga K, Miyazawa N. Diagnosis of mediastinal lymph node metastases in lung cancer. *Jpn J Clin Oncol* 1992;22:35–40.

Ann Thorac Surg
2007;83:312–4

be considered as potentially metastasizing neoplasms. Therefore the benign behavior is probably variable, and the aspects that indicate this behavior need to be clarified.

In summary, the unusual presentation of a benign, clear cell tumor as a large tumor of the lung mimicking malignant behavior in terms of tumor vascularity and local invasion is rare. The need for pneumonectomy for large benign lung tumors is again unusual. The benign behavior is variable, therefore complete surgical resection is probably the best chance to improve survival and quality of life.

References

1. Liebow AA, Castleman B. Benign clear cell tumors of the lung. Am J Pathol 1963;43:13.
2. Gaffey MJ, Mills SE, Zarbo RJ, Weiss LM, Gown AM. Clear cell tumor of the lung. Immnunohistochemical and ultrastructural evidence of melanogenesis. Am J Surg Pathol 1991;15:644–53.
3. Wick MR, Mills SE. Benign and borderline tumors of the lung and pleura. In: Leslie KO, Wick MR, eds. Practical pulmonary pathology a diagnositc approach, 1st ed. Philadelphia: Churchill Livingstone, 2005:713–5.
4. Kung M, Landa JF, Lubin J. Benign clear cell tumor (sugar tumor) of the trachea. Cancer 1984;54:517–9.
5. Alfredo NCS, Flavia SN, Nelson H, Teresa YT. A rare cause of hemoptysis: benign sugar (clear) cell tumor of the lung. Eur J Cardiothorac Surg 2004;25:652–4.
6. Sale GE, Kulander BG. "Benign" clear cell tumor (sugar tumor) of the lung with hepatic metastasis ten years afer resection of pulmonary primary tumor. Arch Pathol Lab Med 1988;112:1177–8.
7. Gaffey MJ, Mills SE, Askin FB, et al. Clear cell tumor of the lung: a clinicopathologic, immunohistochemical and ultrastructural study of eight cases. Am J Surg Pathol 1990;14:248–59.

FEATURE ARTICLES

^{11}C-Acetate and ^{18}F-Fluorodeoxyglucose Positron Emission Tomography of Pulmonary Adenocarcinoma

Masahiro Kaji, MD, PhD, Hiroaki Nomori, MD, PhD, Kenichi Watanabe, MD, PhD, Takashi Ohtsuka, MD, PhD, Tsuguo Naruke, MD, PhD, Keiichi Suemasu, MD, PhD, and Kimiichi Uno, MD, PhD

Department of Thoracic Surgery, Saiseikai Central Hospital, Graduate School of Medicine, Kumamoto University, and Nishidai Clinic, Tokyo, Japan

Positron emission tomography (PET) with ^{11}C-acetate has been recently reported in detection of slow-growing tumors, such as well-differentiated adenocarcinomas of the lung, which are often negative with ^{18}F-fluorodeoxyglucose (FDG) PET. Here we present findings of acetate-PET and FDG-PET in a case of adenocarcinoma that was comprised of peripheral ground glass opacity and solid central components, and was histologically comprised of both a well-differentiated and a moderately-differentiated adenocarcinoma, respectively. Acetate-PET was positive in both components, whereas FDG-PET was only positive in the solid central component. The present case demonstrates the figurative findings of acetate-PET and FDG-PET in lung adenocarcinoma.

(Ann Thorac Surg 2007;83:312–4)

Although positron emission tomography (PET) with ^{18}F-fluorodeoxyglucose (FDG) has contributed significantly to the diagnosis of lung cancers, well-differentiated adenocarcinomas are well known to frequently be falsely negative with FDG-PET, owing to their low rate of glucose metabolism [1]. Recently, we reported that PET with ^{11}C-acetate (AC) was able to detect well-differentiated adenocarcinomas exhibiting a ground-glass opacity (GGO) appearance more frequently than FDG-PET [2]. Here we present the figurative findings of AC-PET and FDG-PET in a case of lung adenocarcinoma that was comprised of peripheral GGO and solid central components that exhibited the histologic characteristics of both a well-differentiated and moderately-differentiated adenocarcinoma, respectively.

The patient was a 76-year-old woman with adenocarcinoma of the left lung that was detected by a routine annual examination. Computed tomography showed a mass shadow (5.5 × 4.5 cm) that consisted of a peripheral GGO component and a solid central component (Fig 1). The size of the solid central compartment was 4.2 × 1.5 cm. The AC-PET and FDG-PET was conducted according to the following protocol. The AC-PET and FDG-PET demonstrated the following findings: the AC-PET was positive in both the solid and GGO components (Fig 2A) and the FDG-PET was positive in the solid component but negative in the GGO (Fig 2B). A left upper lobectomy with mediastinal lymph node dissection was performed on January 11, 2006. Histologic findings revealed that the peripheral GGO component was a well-differentiated adenocarcinoma and that the solid central component was a moderately-differentiated adenocarcinoma.

The ^{11}C-acetate was produced using an HM-18 cyclotron (Sumitomo Heavy Industries Co, Tokyo, Japan) by proton bombardment of $^{14}N_2$. The resultant $^{11}CO_2$ was then reacted with methyl magnesium bromide by a modified method of Pike and colleagues [3]. The AC-PET was performed before FDG-PET on the same day. The dosage of ^{11}C-acetate administered was 125 μCi/kg (4.6 MBq/kg). The PET imaging was performed approximately 10 minutes after the administration of AC using a PosiCam.HZL mPower scanner (Positron Co, Houston, TX). Approximately 30 minutes after AC-PET imaging, fluorine-18 FDG was administered (ie, more than 120 minutes after administration of the AC). The dosage of FDG was 125 μCi/kg (4.6 MBq/kg) for nondiabetic patients and 150 μCi/kg (5.6 MBq/kg) for diabetic patients, as we previously reported [1]. The FDG-PET imaging was performed approximately 45 minutes after administration of the FDG. The cost for one study of AC-PET is less than $100.

Accepted for publication May 16, 2006.

Address correspondence to Dr Kaji, Department of Thoracic Surgery, Saiseikai Central Hospital, 1-4-7, Mita, Minato-ku, Tokyo, 108-0073 Japan; e-mail: mkaji@saichu.jp.

0003-4975/07/$32.00
doi:10.1016/j.athoracsur.2006.05.085

Comment

Recent advances in FDG-PET have contributed significantly to the ability to differentiate between benign and malignant pulmonary nodules. However, FDG-PET sometimes provides false-negative findings, particularly for low-grade malignant tumors, such as bronchioloalveolar carcinoma and carcinoid, due to their low glucose metabolism [1, 4]. We previously reported that while FDG-PET did not exhibit false-negative results for squamous cell, large cell, or small cell carcinomas, 60% of well-differentiated adenocarcinomas (1 to 3 cm in size) failed to be identified by FDG-PET [1].

The ^{11}C-acetate has been widely used as a PET tracer for evaluating myocardial oxidative metabolism [5]. Recently AC-PET has been reported to be a useful PET tracer in detecting slow-growing tumors that have failed to be identified by FDG-PET, such as well-differentiated lung adenocarcinomas, well-differentiated hepatocellular carcinomas, and prostate cancers [2, 6, 7].

It is well known that differentiated adenocarcinomas of the lung are often histologically heterogeneous [8] (ie, in the peripheral zone, tumor cells proliferate in a single layer along the alveolar septa, as in bronchioloalveolar carcinomas; whereas in the central zone, tumor cells proliferate in moderately-differentitated or poorly-differentiated papillary structures along with an increase of fibrovascular stroma). Here we present the findings of AC-PET and FDG-PET in a case of adenocarcinoma that consisted of peripheral GGO and solid central components, which exhibited the histologic characteristics of well-differentiated and moderately-differentiated adenocarcinomas, respectively. Although AC-PET was positive in both components, FDG-PET was only positive in the central component of the moderately-differentiated carcinoma, which are typical findings of AC-PET and FDG-PET.

Fig 1. Computed tomography showing the lesion composed of the peripheral ground glass opacity and the central solid components.

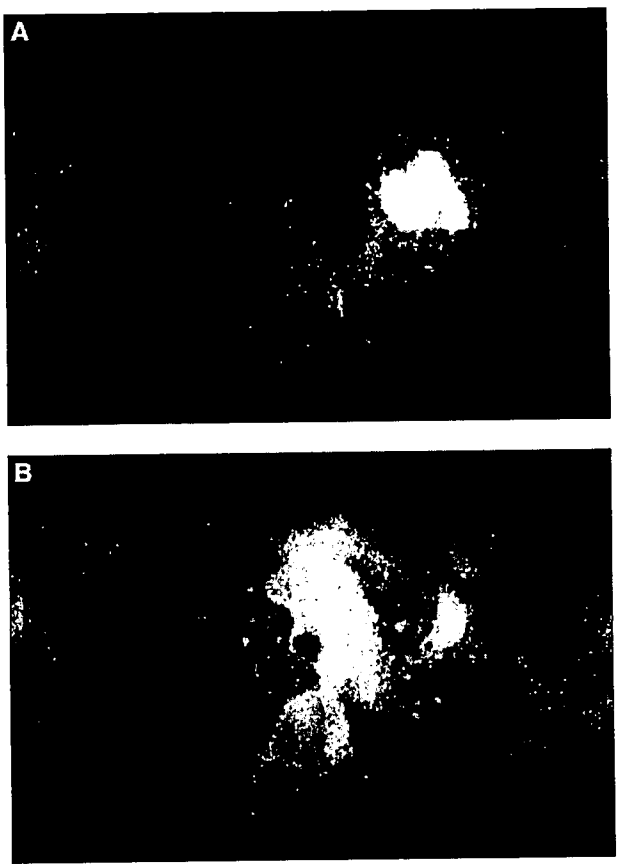

Fig 2. Fusion findings of computed tomography and positron emission tomography. (A) Acetate-positron emission tomography (AC-PET) was positive in both the peripheral ground-glass opacity and the central solid components. (B) The ^{18}F-fluorodeoxyglucose (FDG)-PET was positive in the central solid component but negative in the peripheral ground-glass opacity component.

Our previous investigation demonstrated that 6 of 10 (60%) moderately-differentiated or poorly-differentiated adenocarcinomas were positive with both FDG-PET and AC-PET. Therefore we believe that differentiated adenocarcinomas with GGO images on CT should be examined with AC-PET rather than FDG-PET.

References

1. Nomori H, Watanabe K, Ohtsuka T, et al. Evaluation of F-18 fluorodeoxyglucose (FDG) PET scanning for pulmonary nodules less than 3 cm in diameter, with special reference to the CT images. Lung Cancer 2004;45:19–27.
2. Nomori H, Kosaka N, Watanabe K, et al. ^{11}C-acetate positron emission tomography imaging for lung adenocarcinoma 1 to 3 cm in size with ground-glass opacity images on computed tomography. Ann Thorac Surg 2005;80:2020–5.
3. Pike VW, Eakins MN, Allan RM, et al. Preparation of [1-^{11}C] acetate—an agent for the study of myocardial metabolism by positron emission tomography. Int J Appl Radiat Isot 1982;33:505–12.
4. Nomori H, Watanabe K, Ohtsuka T, et al. Visual and semiquantitative analyses for F-18 fluorodeoxyglucose (FDG) PET scanning in pulmonary nodules 1 to 3 cm in size. Ann Thorac Surg 2005;79:984–8.

Ann Thorac Surg
2007;83:314–5

5. Brown M, Marshall DR, Sobel BE, Bergmann SR. Delineation of myocardial oxygen utilization with carbon-11-labeled acetate. Circulation 1987;76:687–96.
6. C, Yeung DW. C-11 acetate PET imaging in hepatocellular carcinoma and other liver masses. J Nucl Med 2003;44:213–21.
7. Oyama N, Akino H, Kanamaru H, et al. ^{11}C-acetate PET imaging of prostate cancer. J Nucl Med 2002;43:181–6.
8. Shimosato Y, Hashimoto T, Kodama T, et al. Prognostic implications of fibrotic focus (scar) in small peripheral lung cancers. Am J Surg Pathol 1980;4:365–73.

Prolonged Survival Due to Spontaneous Regression and Surgical Excision of Malignant Mesothelioma

John E. Pilling, MRCS, Andrew G. Nicholson, FRCPath, Clive Harmer, FRCP, and Peter Goldstraw, FRCS

Departments of Thoracic Surgery and Pathology, Royal Brompton Hospital, and Department of Oncology, Royal Marsden Hospital, London, United Kingdom

We report a case of malignant pleural mesothelioma with histologically proven spontaneous regression of pleural disease. During a 12-year follow-up there was a single recurrence, which was a lesion in the chest wall at 6 years that was surgically excised. A prominent host response to tumor was seen in both the primary tumor and the recurrence.

(Ann Thorac Surg 2007;83:314–5)

FEATURE ARTICLES

Malignant mesothelioma is an exceptionally aggressive and almost universally fatal neoplasm arising from mesothelial cells that form the serosal lining of the pleural, peritoneal, and pericardial cavities. We report the case of a long-term survivor with malignant pleural mesothelioma (MPM) in which spontaneous regression of the disease has been histologically proven and whose recurrence was controlled with limited surgical excision.

A 58-year-old man presented in 1994 with a 3-month history of chest pain and dyspnea. He was a nonsmoker who had significant occupational exposure to asbestos 16 years previously. Left video-assisted thoracoscopic surgery at another hospital demonstrated a blood stained pleural effusion and tumor nodules infiltrating the posterior parietal pleura. The operative report clearly identified the area of macroscopic disease from which the biopsy was taken. Pleural biopsies showed fibrous thickening with infiltration by a malignant, predominantly epithelioid neoplasm. There were occasional sarcomatoid areas and a prominent inflammatory cell infiltrate. Immunohistochemistry showed a mesothelial phenotype with subsequent diagnosis of MPM. The patient consulted an oncologist, opting for radiological surveillance but no further active treatment at that time.

Five years later he presented with an enlarging, painless chest wall mass 5 cm in diameter overlying the anterior ends of the third to fifth ribs, distant from the previous video-assisted thoracoscopic surgery port sites (Fig 1). A needle biopsy confirmed malignancy and the patient proceeded to a left thoracotomy, multiple pleural biopsies, and chest wall resection with insertion of prosthesis. The chest wall mass was shown to be a completely excised epithelioid MPM in which there was a moderate host inflammatory response (Fig 2). There was a moderately high proliferation index. The mass was arising from the chest wall and was not in continuity with the parietal pleura. It was believed to be a hematogenous metastasis from the original MPM. Both the video-assisted thoracoscopic surgery biopsies and the chest wall lesion were subject to international pathologic review, which confirmed the diagnosis of MPM. Extensive parietal pleurectomy from the region of the previous VATS biopsy in the left paravertebral gutter showed mild fibrosis with no evidence of malignancy. Recovery from the operation was uneventful.

At follow-up 7 years after chest wall resection and 12 years after initial presentation, the patient remains asymptomatic with no radiologic evidence of recurrence. During this time, no adjuvant therapy has been given.

Comment

Survival after diagnosis of MPM is generally poor. Even in those fit for surgical palliation the median survival after surgery is 10 months [1]. Tri-modality therapy (ie, combined radical surgery, radiotherapy and chemotherapy) has had limited success outside of specific subgroups in which patients with epithelioid MPM, negative surgical resection margins, and unaffected extrapleural lymph nodes had a 5-year survival of 46% [2]. Although patients with prolonged survival after very limited treatment have been reported [3], it is extremely rare.

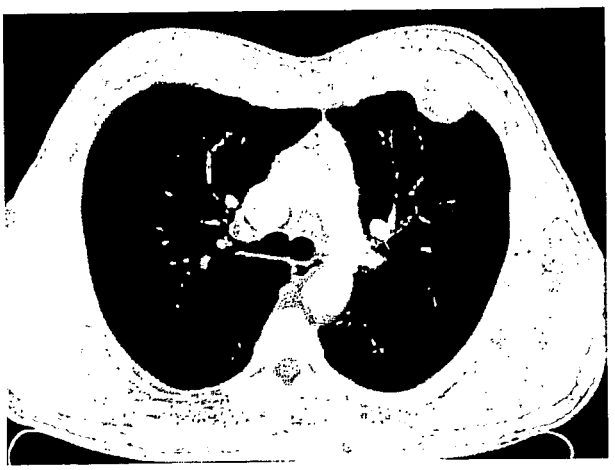

Fig 1. Computed tomographic scan showing chest wall mass at anterior ends of the third to fifth ribs.

Accepted for publication May 15, 2006.

Address correspondence to Prof Goldstraw, Department of Thoracic Surgery, Royal Brompton Hospital, Sydney St, London, SW36NP United Kingdom; e-mail: p.goldstraw@rbh.nthames.nhs.uk.

0003-4975/07/$32.00
doi:10.1016/j.athoracsur.2006.05.070

ONCOLOGY REPORTS 15: 437-442, 2006

Lymphatic microvessel density using D2-40 is associated with nodal metastasis in non-small cell lung cancer

IWAO TAKANAMI

Department of Surgery, Teikyo University School of Medicine, Tokyo, Japan

Received September 6, 2005; Accepted October 28, 2005

Abstract. The monoclonal antibody D2-40 is a new selective marker for lymphatic endothelium. The lymphatic microvessel density (LMVD) using D2-40 has not yet been evaluated in non-small cell lung cancer (NSCLC). The aim of this study was to evaluate LMVD using D2-40 in NSCLC. We investigated LMVD in 77 patients with NSCLC who underwent curative tumor resection. We also determined the relation between LMVD and clinicopathologic factors, VEGF-C and Ang-2 and microvessel density (MVD) using factor VIII-related antigen. The median number of D2-40-positive vessels in the highest LMVD was 25 (range, 5-71). LMVD was significantly associated with tumor status, lymph node metastasis, stage, lymphatic invasion, VEGF-C protein and MVD ($p=0.0149$ for tumor status; $p<0.0001$ for nodal status; $p<0.0001$ for stage; $p=0.0153$ for lymphatic invasion; $p=0.0030$ for VEGF-C, and $p=0.0029$ for MVD). Furthermore, LMVD using D2-40 expression was shown to be an independent predictor of lymph node metastasis by multivariate analysis ($p=0.0070$). These data indicate that a high LMVD by D2-40 may be an indicator of lymph node metastasis in NSCLC.

Introduction

Cancer cell spread to regional lymph nodes is an early event in the progression of many solid tumors, and the lymphatic vasculature serves as the primary route for metastatic spread. Lymphangiogenesis studies have been limited by lack of specific lymphatic endothelial markers. Monoclonal antibody D2-40 was reported to be a selective marker for lymphatic endothelium (1), and has been shown to be useful in identifying the presence of lymphatic invasion in various malignant neoplasms (2). Studies of various tumors have shown the potential clinical significance of lymphangiogenesis, suggesting that lymphatic microvessel density correlates with tumor growth and metastasis (3). The modulation of lymphatic vascular development has been identified, and vascular endothelial growth factor-C (VEGF-C) (4), angiopoietin-2 (Ang-2) (5) and angiogenesis (6) are reported to regulate lymphatic development. The lymphatic microvessel density using D2-40 has not yet been evaluated in non-small cell lung cancer (NSCLC), and it remains to be elucidated whether the lymphatic microvessel density is related to VEGF-C, Ang-2 and blood microvessel density in NSCLC. Thus, we investigated the lymphatic microvessel density using immunohistochemical D2-40 in a series of 77 cases of curatively resected NSCLC for its clinical significance. We also determined whether the lymphatic microvessel density using D2-40 correlates with the immunohistochemical assay of VEGF-C, Ang-2 and blood microvessel density using factor VIII-related antigen (F8RA).

Correspondence to: Dr Iwao Takanami, Department of Surgery, Teikyo University School of Medicine, 11-1 Kaga 2-Chome, Itabashi-Ku, Tokyo 173-8605, Japan
E-mail: takanami@med.teikyo-u.ac.jp

Abbreviations: Ang-2, angiopoietin-2; NSCLC, non-small cell lung cancer; LMVD, lymphatic microvessel density; MVD, microvessel density

Key words: D2-40, immunohistochemistry, non-small cell lung cancer, lymph node metastasis, lymphangiogenesis

Materials and methods

Patients and tumors. Tumor tissue was collected from 77 patients with NSCLC who underwent curative surgery between 1995 and 1999 at the Department of Surgery, Teikyo University School of Medicine. Patients who died within a month after surgery and patients with a past history of another cancer were excluded from the study. Patients were also excluded if they had received neoadjuvant chemotherapy or radiotherapy. The 77 patients included 56 men and 21 women ranging in age between 34 and 84 years (mean, 66.3 years). With regard to histological type, 43 were adenocarcinomas, 31 were squamous cell carcinomas and 3 were large cell lung carcinomas. There were 21 patients with stage IA, 17 patients with stage IB, 1 patient with stage IIA, 14 patients with stage IIB and 24 patients with stage IIIA. Tissue samples to be used for immunohistochemistry and H&E staining were fixed in formalin and paraffin embedded.

Immunohistochemical staining. Immunohistochemical studies of D2-40, F8RA, VEGF-C and Ang-2 were performed, and these specimens were immunostained using formalin-fixed, paraffin-embedded tissues. The sections were immersed for 30 min in 0.3% H_2O_2 in absolute methanol and treated with

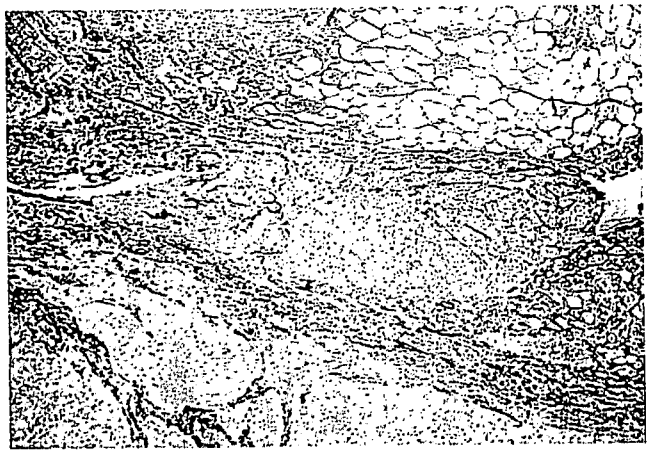

Figure 1. Some D2-40-positive lymphatic vessels are present at the tumor periphery. Original magnification, x15.

Figure 2. D2-40-positive lymphatic vessels. Original magnification, x37.5.

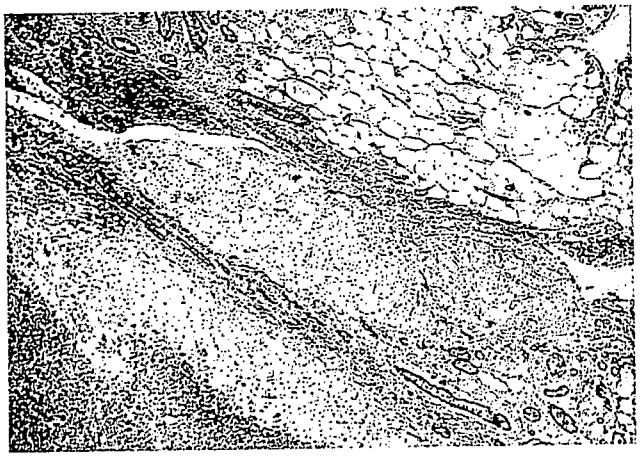

Figure 3. Some F8RA-positive vessels are found in the same tumor. Original magnification, x15.

10% normal rabbit serum. Overnight incubation with the anti-D2-40 monoclonal antibody (Signet Laboratories, Dedham, MA), anti-F8RA monoclonal antibody (Nichirei, Tokyo, Japan), anti-VEGF-C polyclonal antibody (Santa Cruz Biotechnology, CA) and anti-Ang-2 polyclonal antibody (Santa Cruz Biotechnology) was followed by incubation with biotinylated rabbit anti-mouse IgG and biotinylated rabbit anti-goat IgG, respectively, and an avidin-biotin-peroxidase reaction that used 3,3'-diaminobenzidine tetrahydrochloride in the presence of 0.05% H_2O_2. Negative control sections were treated using nonimmunized mouse IgG and goat IgG as the primary antibodies. Normal pulmonary tissue sections were used as positive controls.

Specimen classification based on immunohistochemical results. Two independent observers without knowledge of the patient data simultaneously evaluated the immunohistochemical results. The lymphatic microvessel density and microvessel density were evaluated according to the methods previously described (7). Briefly, after immunostaining with anti-D2-40 antibody and anti-F8RA antibody, the stained sections of D2-40 and F8RA were screened at an original magnification of x100 to identify the regions of highest lymphatic microvessel density and microvessel density. The lymphatic microvessel density and microvessel density were chosen at random and determined in different fields of serial sections. A grid (0.15x0.20 mm) that defined areas of 0.03 mm^2 per field was used to count the lymphatic vessels and microvessels at an original magnification of x400 (x40 objective lens with a x10 eyepiece) in three regions with the highest lymphatic microvessel density and microvessel density. The number of lymphatic vessels and microvessels was determined by averaging three separate counts of each grid made by two observers. The degree of VEGF-C reactivity within individual tissue sections was considered positive if unequivocal staining of carcinoma cells was seen in >10% of the tumor cells; when <10% were stained, the samples was classified as negative in VEGF-C, as previously described (8). For Ang-2 immunohistochemistry, tumor sections were considered positive if >5% of tumor cells were immunoreactive, as previously described (9).

Statistical analysis. All data regarding the clinical and histopathologic variables were stored in a computer. The StatView program (Abacus Concepts, Berkeley, CA, USA) was used for all statistical analyses. Association between the clinicopathological data and expression of D2-40 immunohistochemical expression was analyzed using the Chi-square test and Student's t-test. A stepwise logistic regression model was used for the multivariate analysis. All tests were considered significant when $p<0.05$.

Results

D2-40, F8RA, VEGF-C, and Ang-2 expression in NSCLC. The expression of D2-40 in the lymphatics was confirmed in the bronchial submucosa. The F8RA positive vascular network was slightly noted in alveolar tissues. D2-40 expression was mainly present in thin-walled lymphatic structures (Figs. 1 and 2). D2-40-positive lymphatic vessels were found in all cases. Lymphatic vessels were observed both within the tumor mass and in the peritumoral area or tumor edge. Lymphatic vessels in the peritumoral area or the tumor edge were more numerous and occupied a greater relative area compared with intratumoral lymphatics. The regions with the

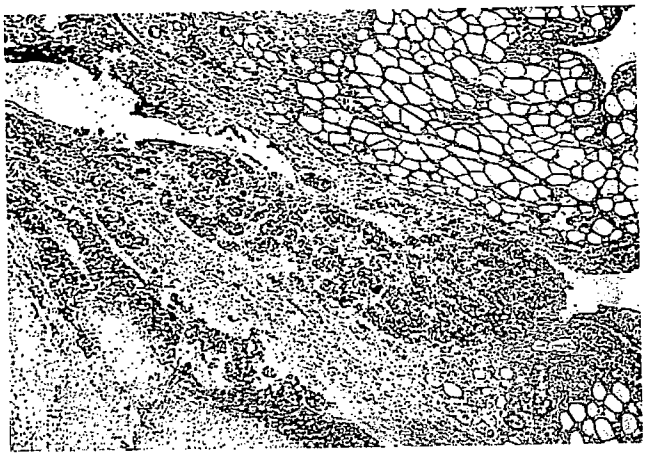

Figure 4. VEGF-C expression in carcinoma cells. Original magnification, x15.

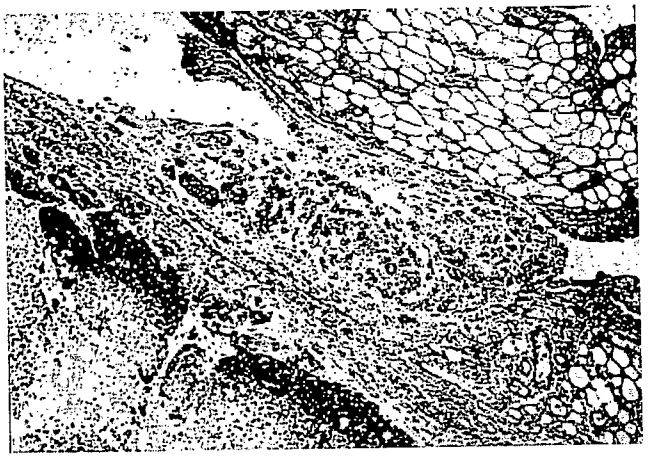

Figure 5. Ang-2 expression in carcinoma cells. Original magnification, x15.

greatest number of D2-40-positive vessels were most frequently the peritumoral area within 500 μm from the tumor border or the margins of the tumor. The median number of D2-40-positive vessels in the highest lymphatic microvessel density was 25 (range, 5-71). The regions of greatest vascularization using F8RA were most frequently apparent at the margins of the tumors, as most of D2-40 vessels were consistently noted (Fig. 3). The median number of F8RA-positive vessels was 15 (range, 5-52). Immunohistochemical assay of VEGF-C and Ang-2 revealed that VEGF-C and Ang-2 were expressed predominantly in cancer tissues (Figs. 4 and 5), and very low expression of VEGF-C and Ang-2 were present in normal tissues. Positive expression of VEGF-C and Ang-2 were primarily seen at the edges of tumor tissues and found in the cytoplasm of tumor cells. Of 77 cases, 46 patients (58.7%) were positive for VEGF-C, and 26 patients (34.2%) were positive for Ang-2.

Association between expression of D2-40, F8RA, VEGF-C, Ang-2 expression and clinicopathological factors. We classified the cases into two subgroups split by median D2-40 count: a low D2-40 density group (n=39) for which D2-40 density was ≤25; and a high D2-40 density group (n=38) for which D2-40 density was >25. Table I shows the clinicopathological parameters for these two groups. There were no significant intergroup differences regarding gender ratio, histology, vascular invasion, and Ang-2 protein. However, D2-40 density was significantly related to the tumor status, lymph node status, stage, lymphatic invasion, VEGF-C and microvessel density (p=0.0149 for tumor

Table I. Association between D2-40 density and various clinicopathological factors in patients with lung cancer.

Variable	D2-40 density low (≤25) (n=39)	D2-40 density high (>25) (n=38)	p-value
Gender			
Male	30	26	
Female	9	12	0.3420
Tumor status			
T1	16	6	
T2	18	19	
T3	5	13	0.0149
Nodal status			
Negative	33	14	
Positive	6	24	<0.0001
Stage			
IA/IB	29	9	
IIA/IIB	5	10	
IIIA	5	19	<0.0001
Lymphatic invasion			
Negative	23	11	
Positive	16	27	0.0153
Vascular invasion			
Negative	24	15	
Positive	15	23	0.0870
Histology			
Adenocarcinoma	21	22	
Squamous cell ca.	17	14	
Large cell ca.	1	2	0.7258
VEGF-C protein			
Negative	22	9	
Positive	17	29	0.0030
Ang-2 protein			
Negative	30	21	
Positive	9	17	0.0765
MVD[a]			
Low (≤15)	29	14	
High (>15)	10	23	0.0029

[a]Microvessel density median, 15; ca, carcinoma.

Table II. Statistical associations between lymph node metastasis and examined variables.

Variables	Lymph node metastasis		Univariate p-value	Multivariate p-value
	Negative (n=47)	Positive (n=30)		
Tumor status				
T1	19	3		
T2	19	18		
T3	9	9	0.0010	0.4404
Lymphatic invasion				
Negative	29	5		
Positive	18	25	0.0003	0.0340
Vascular invasion				
Negative	30	9		
Positive	17	21	0.0077	0.4337
VEGF-C protein				
Negative	25	6		
Positive	22	24	0.0078	0.7024
Ang-2 protein				
Negative	35	16		
Positive	12	14	0.0952	0.7448
MVD				
Low (≤15)	32	14		
High (>15)	15	16	0.1023	0.2025
LMVD				
Low (≤25)	33	6		
High (>25)	14	14	<0.0001	0.0070

status; $p<0.0001$ for nodal status; $p<0.0001$ for stage; $p=0.0153$ for lymphatic invasion; $p=0.0030$ for VEGF-C, and $p=0.0029$ for microvessel density).

Associations between lymph node metastasis and examined variables. The independent predictors of lymph node metastasis were determined using stepwise logistic regression analysis. As shown in Table II, T factor, lymphatic invasion, vascular invasion, VEGF-C protein and the lymphatic microvessel density were correlated with lymph node metastasis by univariate analysis. According to the multivariate analysis of these variables, lymphatic invasion and the lymphatic microvessel density proved to be the predictors of lymph node metastasis ($p=0.0340$ for lymphatic invasion and $p=0.0070$ for lymphatic microvessel density).

Discussion

NSCLC is a leading cause of morbidity and mortality among men and women in the U.S. (10). Despite major advances in cancer treatment in past 2 decades, the prognosis of patients with lung cancer has improved only minimally (10). Lymph node metastasis is one of the most powerful prognostic markers for resected NSCLC (11). Tumor cell spread via lymphatic capillaries is an early feature of many carcinomas. Evidence of the formation of lymphatic capillaries (lymph-angiogenesis) has raised the possibility that cells within primary tumors can contribute actively to lymphatic dissemination through the induction of a lymphangiogenic process. Studies on lymphangiogenesis rely on the use of specific markers of lymphatic endothelial cells. D2-40 antibody was reported to detect a fixation-resistant epitope on a 40-kDa O-linked sialoglycoprotein expressed in lymphatic endothelium, but not blood vessels (2). D2-40 immuno-reactivity appears to be an appropriate marker to assess lymphangiogenesis. Microvessel density, which presents an estimate for tumor angiogenesis, has been associated with metastatic spread and/or prognosis in individuals with NSCLC (12). However, the lymphatic microvessel density using D2-40 has not yet been widely evaluated.

In this study, most of the D2-40-positive vessels were found to be located in the peritumoral area or at the tumor edge. Previous studies present evidence that the center of tumors do not contain functional lymphatics, however, the lymphatic vessels at the tumor margins do facilitate lymphatic spread of tumor cells (13). The high lymphatic microvessel density at the margins of the tumor is thought to indicate the probability of lymphatic metastasis (13). D2-40

immunoreactivity did not show any association with various clinicopathological tumor features including gender, vascular invasion, and histology in our study. On the other hand, high levels of D2-40 immunoreactivity were significantly associated with tumor status, advanced stage, the presence of lymphatic invasion and lymph node metastasis. Our results are concordant with a previous study reporting that D2-40 lymphatic microvessel density correlated with tumor stage and lymph node metastasis in breast carcinoma (14). Bono *et al* also reported the significant association between the number of Lyve-1-positive vessels and lymph node metastasis (15).

The lymphatic microvessel density using D2-40 did not show any association with the expression of Ang-2 protein, but the lymphatic microvessel density had a significant association with VEGF-C and the microvessel density in our study. VEGF-C, a novel VEGF member, has been found to introduce not only angiogenesis but also lymphangiogenesis via VEGF-R2 and VEGF-R3 (16). VEGF-C appears to be an important lymphangiogenic factor, and the correlation of VEGF-C expression with lymph node metastasis has been reported in many malignant tumors (17,18). VEGF-C may exert a more powerful effect to enhance lymphangiogenesis and facilitate lymphatic dissemination of tumor cells. Lymph-angiogenesis appears to frequently accompany angiogenesis (19). The discovery of Ang-1 and Ang-2 has provided novel and important insights into the molecular mechanisms of blood vessel formation. Ang-2 is required for vascular remodeling during angiogenesis. The remodeling phase is crucial for the proper organization of new vessels, and it seems likely that a similar remodeling step occurs in lymph-angiogenesis. The Ang-2 knockout perinatal mouse showed defects in the overall organization of their lymphatic vasculature, and Ang-2 was thought to relate to lymphatic vessel formation or lymphangiogenesis (20). A correlation between lymph node involvement and Ang-2 expression was found in colon and breast carcinomas (21,22), but is controversial (23). VEGF and/or VEGF-C expression was reported to be present in tumors overexpressing Ang-2 (22). Another study, however, presents that VEGF-C plays a role in the early stage of lymphatic vessel formation, and Ang-2 plays a role in the later remodeling stages (20). Our results that lymphatic microvessel density did not show an association with the expression of Ang-2 protein, but lymphatic micro-vessel density had a significant association with VEGF-C may be in accordance with results of this previous study. Lymphangiogenesis is often seen together with angiogenesis because newly emerging blood vessels are leaky and need lymphatic growth to avoid tissue edema (23). A significant correlation between lymphangiogenesis and angiogenesis was found in this study.

Tumor state, vascular invasion and VEGF-C protein were not detected as being independent factors for lymph node metastasis by multivariate analysis. Multivariate analysis demonstrated that lymphatic invasion and the lymphatic microvessel density were independent factors for lymph node metastasis, with the lymphatic microvessel density found to be the most powerful independent factor. As VEGF-C was dependent on the lymphatic microvessel density, VEGF-C may statistically interfere with the lymphatic microvessel density on lymph node, and VEGF-C was not an independent factor for lymph node metastasis. In our study, a significant difference in the rate of patient survival was detected between patients whose tumors had high lymphatic microvessel density compared to those whose tumors had low lymphatic micro-vessel density. Multivariate analysis demonstrated that the lymphatic microvessel density was an independent factor for overall survival (data not shown). But the number of patients in our study was small, and further studies may be needed to broadly evaluate these findings.

In conclusion, this study showed that the lymphatic microvessel density using D2-40 was elevated in advanced NSCLC, and this elevation is likely the result of elevated levels of expression of lymphangiogenic factors and their specific receptor. Tumors with a high D2-40 vessel density are associated with lymph node metastasis compared with tumors with a low density. In multivariate analysis, D2-40 was shown to be the predictor for lymph node metastasis. Further studies are required to fully understand the role of D2-40 in the lymphatic development in NSCLC, which may represent a future target for new therapeutic strategies.

References

1. Marks A, Sutherland DR, Bailey D, *et al*: Characterization and distribution of an oncofetal antigen (M2A antigen) expressed on testinal germ cell tumors. Br J Cancer 80: 569-578, 1999.
2. Kahn HJ and Marks A: A new monoclonal antibody, D2-40, for detection of lymphatic invasion in primary tumors. Lab Invest 82: 1255-1257, 2002.
3. Nisato RE, Tille JS and Pepper MS: Lymphangiogenesis and tumor metastasis. Thromb Haemost 90: 591-597, 2003.
4. Jeltsch M, Kaipainen A, Joukov V, *et al*: Hyperplasia of lymphatic vessels in VEGF-C transgenic mice. Science 276: 1423-1425, 1997.
5. Maisonpierre PC, Suri C, Jones PF, *et al*: Angiopoietin-2 is required for postnatal angiogenesis and lymphatic patterning, and only the latter role is resqued by angiopoietin-1. Dev Cell 3: 411-423, 2002.
6. Takahashi M, Yoshimoto T and Kubo H: Molecular mechanisms of lymphangiogenesis. Int J Hematol 80: 29-34, 2004.
7. Takanami I, Takeuchi K and Naruke M: Mast cell density is associated with angiogenesis and poor prognosis in pulmonary adenocarcinoma. Cancer 88: 2686-2692, 2000.
8. Hoar FJ, Chaudri S, Wadley MS and Stonelake PS: Co-expression of vascular endothelial growth factor C (VEGF-C) and c-erb B2 in human breast carcinoma. Eur J Cancer 39: 1698-1703, 2003.
9. Tanaka F, Ishikawa K, Yanagihara K, *et al*: Expression of angiopoietins and its clinical significance in non-small cell lung cancer. Cancer Res 62: 7124-7129, 2002.
10. Ginsberg R, Vokes E and Raben A: Non-small cell lung cancer. In: Cancer: Principles and Practice of Oncology. DeVitaV Jr, Helleman S and Rosenberg S (eds). Lippencott-Raven, Philadelphia, pp858-911, 1997.
11. Naruke T, Goya T, Tsuchiya R and Suematsu K: Prognosis and survival in resected lung carcinoma based on the international staging system. J Thorac Cardiovasc Surg 96: 440-447, 1998.
12. Macchiarini P, Fontaini G, Hardlin MJ, Squantini F and Angellitti GA: Regulation of neovasculisation to metastasis of non-small cell lung cancer. Lancet 340: 145-146, 1992.
13. Padera TP, Kadambi A, DiThomaso E, *et al*: Lymphatic metastasis in the absent of functional intratumoral lymphatics. Science 296: 1883-1886, 2002.
14. Choi WWL, Lewis M, Lawson D, *et al*: Angiogenic and lymph-angiogenic microvessel density in breast carcinoma: correlation with clinicopathologic parameters and VEGF-family gene expression. Modern Pathol 18: 143-152, 2005.
15. Bono P, Wasenius VM, Heikkila P, Lundin J, Jackson DG and Joensuu H: High Lyve-1 positive lymphatic vessel numbers are associated with poor outcome in breast cancer. Clin Can Res 10: 7144-7149, 2004.

16. Cao Y, Linden P, Farnebo J, *et al*: Vascular endothelial growth factor C induces angiogenesis *in vivo*. Proc Acad Sci USA 85: 14389-14394, 1998.
17. Sendivy R, Beck-Managetta J, Haverkampf C, Battistutti W and Henigschnabel S: Expression of vascular endothelial growth factor-C correlates with lymphatic microvessel density and the nodal status in oral squamous cell cancer. Oral Pathol Med 32: 4555-4560, 2003.
18. Niki T, Iba S, Tokunou M, Yamada T, Matsuno Y and Hirohashi S: Expression of vascular endothelial growth factor A, B, C, and D and theirrelationship to lymph node status in lung adenocarcinoma. Clin Cancer Res 6: 2431-2439, 2000.
19. Alitalo K and Carmeliet P: Molecular mechanisms of lymph-angiogenesis in health and disease. Cancer Cell 1: 219-227, 2002.
20. Oki Y, Yasunaga K, Ito Y, *et al*: Angiopoietin-related growth factor (AGF) promotes epidermal proliferation, remodeling, and regeneration. Proc Natl Acad Sci USA 100: 9494-9499, 2003.
21. Ochiumi T, Tanaka S, Oka S, *et al*: Clinical significance of angiopoietin-2 expression at the deepest invasive tumor site of advanced colorectal carcinoma. Int J Oncol 24: 539-547, 2004.
22. Sfiligoi C, deLuca AD, Cascone I, *et al*: Angiopoietin-2 expression in breast cancer correlates with lymph node invasion and short survival. Int J Cancer 103: 466-474, 2003.
23. Sun XD, Liu XE, Wu JM, Cai XJ, Mou YP and Li JD: Expression and significance of angiopoietin-2 in gastric cancer. World J Gastroenterol 10: 1382-1385, 2004.
24. Thurston G: Role of angiopoietins and Tie receptor tyrosine kinases in angiogenesis and lymphangiogenesis. Cell Tissue Res 314: 61-68, 2003.

Brief Report

Dissimilarity in Gene Expression Profiles of Lung Adenocarcinoma in Japanese Men and Women

Junichi Okamoto, MD[1,2]; Masamitsu Onda, MD, PhD[2]; Tomomi Hirata, MD, PhD[1]; Shizuyo Miyamoto, MS[2]; Junko Akaishi, MD[1,2]; Iwao Mikami, MD, PhD[1]; Kyoji Hirai, MD, PhD[1]; Shuji Haraguchi, MD, PhD[1]; Kiyoshi Koizumi, MD, PhD[1]; and Kazuo Shimizu, MD, PhD[1]

[1]Department of Surgery II, Nippon Medical School, Tokyo, Japan; and [2]Department of Molecular Biology, Institute of Gerontology, Nippon Medical School, Kawasaki, Japan

ABSTRACT

Background: Although clinical differences in lung cancer between men and women have been noted, few studies have examined the sex dissimilarity using gene expression analysis.

Objective: The purpose of this study was to determine the different molecular carcinogenic mechanisms involved in lung cancers in Japanese men and women.

Methods: Patients who received surgery for stage I lung adenocarcinoma were included. RNA was extracted from cancerous and normal tissue, and gene expression was then examined with oligonucleotide microarray analysis. A quantitative polymerase chain reaction assay was performed.

Results: In a microarray analysis of tissue from 13 men and 6 women, 12 genes were underexpressed and 24 genes were overexpressed in lung adenocarcinoma in women compared with men. Genes related to cell cycle were present in underexpressed genes, and genes related to apoptosis, ubiquitination, and metabolism were observed in overexpressed genes. Of interest among the selected genes were WAP four-disulfide core domain 2 (*WFDC2*) and major histocompatibility complex, class II, DM alpha (*HLA-DMA*); these genes were classified into 2 groups by hierarchical clustering analysis. Expression of *WFDC2* in nonsmokers was significantly higher than that in smokers (P = 0.023). However, there was no significant difference in *HLA-DMA* expression between smokers and nonsmokers.

Conclusion: Thirty-six genes that characterize lung adenocarcinoma by sex were selected. This information may contribute to the development of novel diagnostic techniques and treatment modalities that consider sex differences in lung adenocarcinoma. (*Gend Med.* 2006;3:223–235) Copyright © 2006 Excerpta Medica, Inc.

Key words: lung adenocarcinoma, gender, expression, oligonucleotide microarray.

Accepted for publication March 21, 2006.

1550-8579/06/$19.00

INTRODUCTION

Lung cancer is a main cause of malignancy-related death around the world. Biologically, lung cancer has uniquely characteristic epidemiology and histology, for example, in the difference in incidence between men and women. It is estimated that the incidence of lung cancer in females is one third that of males.[1] In addition, most lung cancers in women are adenocarcinomas; in Japanese women, the predominant histological types are adenocarcinoma (73%) and squamous cell carcinoma (12%),[2] and in Spanish women, the predominant types are adenocarcinoma (56.2%), squamous cell carcinoma (8.2%), and large cell carcinoma (2.7%).[3] Women who smoke are more likely than men to develop adenocarcinoma of the lung,[4,5] even though more histological types of lung cancer, for example, squamous cell carcinomas, occur in male smokers. These epidemiological facts suggest that there might be sex differences in the molecular carcinogenic mechanism of male and female lung cancer.

Recently, a novel molecular targeted drug, gefitinib, has been developed. Gefitinib is an epidermal growth factor receptor (EGFR)–tyrosine kinase inhibitor[6] that, interestingly, was reported to be especially effective in Japanese or Asian women with lung adenocarcinoma.[7] Inhibition of EGFR mutation is an important factor in gefitinib's effectiveness against lung cancer,[8] but it is still unknown why gefitinib is effective for female, and especially Asian, lung adenocarcinoma.

To investigate the difference between male and female lung adenocarcinoma in Japanese patients on the molecular level, we examined gene expression profiles using oligonucleotide microarrays. We believe, based on our search of the PubMed database with no specified time parameters using the search terms *gender, expression profile,* and *lung cancer,* that this is the first report focused on the gene expression profile of male and female lung adenocarcinomas that offers clues about epidemiologic sex differences. Furthermore, this study may provide useful information for the development of novel molecular targeted medicines.

PATIENTS AND METHODS

Study Population

The patients included in this study received their diagnosis at Nippon Medical School hospitals between 1999 and 2004. Inclusion criteria for patients were primary lung adenocarcinoma, tumor stage IA or IB, and surgery as initial treatment. Demographic and tumor-specific information collected included age, sex, smoking habits, Brinkman index, histological diagnosis, grade of tumor differentiation, and tumor stage. Histological diagnosis and differentiation grade were assigned in accordance with the World Health Organization criteria for lung and pleural tumors.[9] All patients gave informed consent before surgery, and dissected samples were frozen immediately after surgery and stored at –80°C. The study protocol was approved by the hospital study committee.

RNA Extraction, cDNA Synthesis, and Amplification of RNA

RNA extraction, cDNA synthesis, and amplification of RNA to generate a hybridization probe for the microarray were performed as described previously,[10] with some modifications.

Frozen tissues were homogenized in the presence of TRIzol reagent (Invitrogen Corporation, Carlsbad, California), and total RNA was extracted from cancerous and normal tissues according to the manufacturer's instructions. One-microgram aliquots of the extracted RNA were electrophoresed on 3.0% formaldehyde-denaturing gels in the usual manner (samples with 28S/18S ratios >1.5 were selected for subsequent purification) to eliminate degenerated RNA. RNeasy kits (QIAGEN, Valencia, California) were used for purification of RNA. Using 5 μg of each RNA as a template, cDNAs were synthesized in the usual manner. Briefly, the template was mixed with 1 μL of oligo $dT_{12\text{-}18}$ (Invitrogen Corporation) used for annealing primer and denatured at 70°C for 10 minutes before addition of 200 U of reverse transcriptase II (Wako-Junyaku, Osaka, Japan) reaction buffer, 40 U of RNase inhibitor (Wako-Junyaku), and deoxyribonucleotides. Lastly, this mixture was incubated with 2 U of RNase (Wako-Junyaku) at 37°C for 20 minutes.

RNA amplification, labeling, and fragmentation of the probe 2 μg of RNA were completed using a MessageAmp aRNA amplification kit (Ambion, Inc., Austin, Texas) with modifications. Namely, at the in vitro transcription step, 5-(3-aminoallyl)-dUTP (37.5 mM, Ambion, Inc.) and T7 UTP solution (37.5 mM) was used instead of 75 mM T7 UTP solution. This procedure made antisense amplified RNA (aRNA). Eight-microgram samples of aRNA from cases and controls were labeled with Cy3 and Cy5 mono NHS ester, respectively (Amersham Biosciences UK, Buckinghamshire, United Kingdom), by the amino allyl labeling method as described previously.[11] All samples from cases and controls were labeled with both fluorescent dyes for dye-swap microarray experiments.[12]

The fluorescent-labeled aRNAs from cases and controls were mixed equally and concentrated to 32 μL by centrifuging with a Microcon YM-30 (Millipore, Tokyo, Japan). Then, 8 μL of 5x fragmentation buffer (Hitachi Software Engineering Co. Ltd., Tokyo, Japan) was added, incubated at 96°C for 15 minutes, and then immediately placed on ice. After incubation, the probe mixture was concentrated to 15.5 μL by centrifuging with the Microcon YM-10.

Hybridization to AceGene Microarray

AceGene human oligo chip 30K 1 chip version (Hitachi Software Engineering Co. Ltd.) was applied. A hybridization mixture consisted of 15.5 μL of probe mixture, 12.5 μL of 20x SSC, 10 μL of hybridization solution (Hitachi Software Engineering), 4 μL of 50x Denhardt's solution (Wako Pure Chemical Industries, Ltd., Osaka, Japan) and 2.5 μL of 10% SDS. This hybridization mixture was incubated at 96°C for 2 minutes and immediately placed on ice. Then, 0.5 μg of sonicated salmon sperm DNA (Wako Pure Chemical Industries, Co. Ltd.) and 5 μL formamide were added.

The probe was preincubated to 42°C and applied to the AceGene human oligo chip 30K 1 chip version, placed into the hybridization cassette (Hitachi Software Engineering Co. Ltd.), and then incubated at 42°C for 18 hours within a CHBIO computer-controlled thermal incubator (Hitachi Software Engineering Co. Ltd.). After hybridization, the microarray slide was sequentially washed with 2x SSC/0.1% SDS, 2x SSC, and 1x SSC, respectively, for 5 minutes. The temperature of these washing solutions was 30°C.

Selection of Significantly Affected Genes

The signal from each spot was then normalized by a local normalization method.[10–13] Briefly, LOWESS (locally weighted scatterplot smoothing) normalization was performed in every 26 × 25 subgrids, but before this normalization procedure, spots that had a low signal-to-noise ratio of <2.0 were eliminated from further analysis. For replicating filtering of dye-swap experiments, the signal was selected on the basis of a 2-SD cut on the replicates, and then a geometric mean was used as the value of the signal.[14] After normalization of the signal, the signal for gene A was calculated as follows:

$$S_A = \log_2\left\{\left(\frac{\text{Cy5\_case}}{\text{Cy3\_cont}}\right)\times\left(\frac{\text{Cy5\_cont}}{\text{Cy3\_case}}\right)\right\}$$

where *Cy5_case* is the normalized signal of lung cancer samples labeled with Cy5 dye; *Cy3_cont* is the normalized signal of healthy lung samples labeled with Cy3 dye; *Cy5_cont* is the normalized signal of healthy lung samples labeled with Cy5 dye; and *Cy3_case* is the normalized signal of lung cancer samples labeled with Cy3 dye. Then, the average S_A of all genes (S_{A_ave}) and the SD of S_A of all genes (S_{A_SD}) were calculated. Next, the *z* score of each gene A was computed using the equation:

$$Z_A = (S_A - S_{A\_ave})/S_{A\_SD}.$$

Samples that had *z* scores >2 and showed a reversed signal between (Cy5_case/Cy3_cont) and (Cy3_case/Cy5_cont) were eliminated from further analysis. Within the samples that passed the filtering, the gene expression ratio of gene A (R_A) was calculated as:

$$R_A = \frac{\sqrt{(\text{Cy5\_case})\times(\text{Cy3\_case})}}{\sqrt{(\text{Cy5\_cont})\times(\text{Cy3\_cont})}}$$

On filtering these selections, genes were chosen whose expression was either reduced by one

half less than that of the control or upregulated by twice that of the control. After statistical analysis, we selected genes that were over- or underexpressed in female compared with male lung adenocarcinomas.

Hierarchical Clustering Analysis

Average linkage hierarchical clustering was performed using Cluster and TreeView software (Stanford University, Stanford, California).[15]

Real-Time Quantitative Polymerase Chain Reaction Analysis

We performed real-time quantitative polymerase chain reaction (Q-PCR) analysis to evaluate the expression of genes that were selected.[16,17] Q-PCR was carried out with qPCR Mastermix for Syber Green I (Eurogenetec, Seraing, Belgium), and with an ABI 7700 (Applied Biosystems, Foster City, California) as described previously.[10] Primer sequences for β-actin were: 5'-CAAGAGATGGCCACGGCTGCT-3' (forward) and 5'-TCCTTCTGCATCCTGTCGGCA-3' (reverse). Sequence information for genes was collected from the National Center for Biotechnology Information GenBank,[18] and specific primers were designed with the Primer3 software (Whitehead Institute, Cambridge, Massachusetts). Primers are listed in **Table I**. Templates were made from each of the 9 patients who had lung adenocarcinoma only, and mixed normal lung cDNA was obtained from 10 patients (data not shown). Measurements were done in triplicates.

The difference in expression between healthy lung tissue and sample x in lung adenocarcinoma was defined as follows:

$$\Delta Ct_{Xave} = (Ct_{geneX} - Ct_{\beta\text{-actin}})/3,$$

where $Ct_{geneX,\beta\text{-actin}}$ are threshold cycles for amplification of *gene X* and *β-actin*, respectively. Similarly,

$$\Delta Ct_{Nave} = (Ct_{geneX,N} - Ct_{\beta\text{-actin},N})/3,$$

where $Ct_{geneX,N,\beta\text{-actin},N}$ are threshold cycles for amplification of *gene X* and *β-actin* in normal (N) lung, respectively (cDNA was from 10 patients' healthy lung mixture). Expression ratio of *gene X* to healthy lung tissue = $2^{(-\Delta\Delta Ct_x)}$, where

$$\Delta\Delta Ct_X = \Delta Ct_{Xave} - \Delta Ct_{Nave}.$$

Statistical Analysis

Male and female groups were compared using *t*, χ^2, and Fisher exact tests. For microarray analysis, a 1-way analysis-of-variance Welch *t* test and a Mann-Whitney test for unpaired comparison of the 2 groups were applied. These analyses yielded hazard ratios, 95% CIs, and *P* values. *P* values of <0.05 were considered significant.

RESULTS

Patients

The clinical characteristics of the patients studied (13 men, 6 women) are summarized in **Table II**. The median (SD) age of the patients who underwent surgery was 66.53 (14.14) years for men and 63.16 (15.01) years for women. Histopathologic observations included well-differentiated adenocarcinoma (4 men, 4 women), moderately differentiated (2 men, no women), poorly differentiated (6 men, no women), and unknowns (1 man, 2 women). Eleven men and 1 woman were smokers; 2 men and 5 women did not smoke. The median (SD) Brinkman

Table I. Primers for quantitative polymerase chain reaction analysis.

Accession No.	Gene Name	Forward Primer	Reverse Primer
NM_006103	*WFDC2*	AGCAGAGAAGACTGGCGTGT	CCTCCTTATCATTGGGCAGA
NM_006120	*HLA-DMA*	GCCCAACACTTTGGTCTGTT	GTCCATCGACAGCTGAGACA

WFDC2 = WAP four-disulfide core domain 2; *HLA-DMA* = major histocompatibility complex, class II, DM α.

Table II. Association of clinical variables with tumor stage and differentiation in men and women with lung adenocarcinoma.

Clinical Variables	Men (n = 13)	Women (n = 6)	P
Age, y			
Median (SD)	66.53 (14.14)	63.16 (15.01)	NS
Range	47–84	43–80	
Tumor stage,* no. (%) of patients			
IA	7 (53.8)	4 (66.7)	NS
IB	6 (46.2)	2 (33.3)	
Pathological tumor differentiation, no. (%) of patients			
Well	4 (30.8)	4 (66.7)	NS
Moderate	2 (15.4)	0	
Poor	6 (46.2)	0	
Unknown	1 (7.7)	2 (33.3)	
Smoking, no. (%)			
Yes	11 (84.6)	1 (16.7)	NS
No	2 (15.4)	5 (83.3)	
Brinkman index†			
Median (SD)	853.8 (160.4)	41.6 (41.7)	0.037
Range	0–2000	0–250	

NS = not significant.
*World Health Organization criteria.
†Brinkman index = no. of cigarettes/d × years of smoking.

index was 853.8 (160.4) (range = 0–2000) in male patients and 41.6 (41.7) (range = 0–250) in female patients (Brinkman index = no. of cigarettes/d × years of smoking). Other than smoking, there were no significant characteristics shared by men and women.

Differentially Expressed Gene in Lung Adenocarcinoma in Women

The Welch's *t* and Mann-Whitney tests revealed 12 genes that were underexpressed in lung adenocarcinoma in women compared with men. The list of these genes is provided in **Table III**. The expression levels in women varied from 0.69 to 0.54 compared with the expression of adenocarcinoma in men. Nine of these genes have suggested functions. Of note, the proliferating cell nuclear antigen (PCNA) gene showed 0.57-fold less expression in adenocarcinoma in women than in men. In addition, α-tubulin was underexpressed in female cancer, 0.66-fold less than that in male adenocarcinoma.

On the other hand, 24 genes were overexpressed in female lung adenocarcinoma. This list of genes is summarized in **Table IV**. The differences of fold changes in female compared with male adenocarcinoma varied from 2.40 to 1.42. With regard to gene functions, apoptosis (*RNF34*),[19] ubiquitination (*NFKBIB*),[20] and metabolism (*COVA1*)[21] were considered. WAP four-disulfide core domain 2 (*WFDC2*) and major histocompatibility complex, class II, DM alpha (*HLA-DMA*) were also overexpressed.

Hierarchical Clustering

A gene expression portrait of all significant 36 genes with altered expression is shown in **Figure 1**. Unsupervised hierarchical clustering based on $\log_2$ transformation of relative expression values of 36 genes was also classified into a cluster tree with 2 major subgroups.

Real-Time Q-PCR Analysis

A Q-PCR analysis was performed with male and female patients using 2 selected genes:

Table III. List of underexpressed genes in lung adenocarcinoma in women compared with men.

Accession No.	Gene Name	Location	Function Summary	Fold Change*
NM_002157	Heat shock 10kDa protein 1 (chaperonin 10) (*HSPE1*)	2q33.1	Chaperonin 10; interacts with chaperonin 60 (*HSPD1*) to refold denatured proteins; very strongly similar to murine *HSPE1*	0.54
NM_002592	Proliferating cell nuclear antigen (*PCNA*)	20pter-p12	Proliferating cell nuclear antigen; processivity factor for DNA polymerases δ and ϵ	0.57
AC090844	Ensemble Genscan prediction	Unknown	Unknown	0.58
NM_024778	LON peptidase N-terminal domain and ring finger 3 (*LONRF3*)	Xq24	The protein encoded by this gene contains a ring finger domain, a motif present in a variety of functionally distinct proteins and known to be involved in protein-protein and protein-DNA interactions	0.63
NM_001024	Ribosomal protein S21 (*RPS21*)	20q13.3	This gene encodes a ribosomal protein that is a component of the 40S subunit; the protein belongs to the S21E family of ribosomal proteins	0.64
NM_003092	Small nuclear ribonucleoprotein polypeptide B′ (*SNRPB2*)	20p12.2-p11.22	U2 small nuclear RNA-associated protein B″	0.64
NM_006325	RAN, member Ras oncogene family (RAN)	12q24.3	Member of the Ras family of GTP binding proteins; couples DNA synthesis completion to mitosis; induces spindle formation; involved in nuclear transport of RNA and proteins; interacts with polyglutamate repeats of the androgen receptor	0.66
NM_006082	Tubulin, α, ubiquitous (*K-ALPHA*)	12q13.12	Unknown	0.67
NM_033251	Ribosomal protein L13 (*RPL13*)	16q24.3	Ribosomal protein L13; component of the 60S ribosomal subunit	0.67
NM_001005	Ribosomal protein S3 (*RPS3*)	11q13.3-q13.5	Ribosomal protein S3; component of the small 40S ribosomal subunit	0.68
NM_053275	Ribosomal protein, large, P0 (*RPLP0*)	12q24.2	Ribosomal protein P0; acidic phosphoprotein component of the large 60S ribosomal subunit	0.68
NM_002512	Nonmetastatic cells 2 (*NME2*)	17q21.3	Unknown	0.69

*The fold change is the difference in gene expression between women and men.

WFDC2 and *HLA-DMA*. Expression of these genes was significantly higher in women than in men: for *WFDC2*, $P = 0.004$ (Figure 2A); and for *HLA-DMA*, $P = 0.011$ (Figure 2B). Figure 2C shows Q-PCR analysis with smoking as a differentiating factor. Interestingly, expression of *WFDC2* in nonsmokers was significantly higher than that in smokers, but there was no significant difference in *HLA-DMA* expression between smokers and nonsmokers.

DISCUSSION

Although previous studies provided gene expression of lung cancer, they neglected to make a sexual distinction. Harari and Huang[22] insisted that "the assumption that most advanced solid

Table IV. List of overexpressed genes in lung adenocarcinoma in women compared with men.

Accession No.	Gene Name	Location	Function Summary	Fold Change*
NM_006120	Major histocompatibility complex (MHC), class II, DM α (*HLA-DMA*)	6p21.3	α Chain of heterodimer associated with MHC class II molecules; facilitates the binding of peptides to MHC class II molecules	2.40
AC069227	Homo sapiens 12 BAC RP11-478G16	Unknown	Unknown	2.32
AC007610	Ensemble Genscan prediction	Unknown	Unknown	2.06
AF116720	PRO3015	Unknown	Unknown	1.87
BC000845	Unknown (protein for image 3457769)	Unknown	Unknown	1.69
NM_133640	Surfeit 5 (*SURF5*)	9q34.2	Cytoplasmic hydrophilic member of the surfeit family of proteins	1.64
NM_019558	Homeobox D8 (*HOXD8*)	2q31.1	Homeobox D8	1.61
AL356433	Ensemble Genscan prediction	Unknown	Unknown	1.60
NM_006103	WAP four-disulfide core domain 2 (*WFDC2*)	20q12-q13.2	Epididymis-specific secreted protein; may have a role in sperm maturation; may belong to a family of extracellular proteinase inhibitors	1.60
NM_006375	Cytosolic ovarian carcinoma antigen 1 (*COVA1*)	Xq25-q26.2	Cytosolic protein expressed in ovarian carcinoma cells that express the surface glycoprotein CAK1	1.56
NM_025126	Ring finger protein 34 (*RNF34*)	12q24.31	This protein can be cleaved by caspase-3 during the induction of apoptosis	1.56
NM_194252	Tubulin tyrosine ligase-like family, member 11 (*TTLL11*)	9q33.2	Unknown	1.55
NM_013267	Glutaminase 2 (liver, mitochondrial) (*GLS2*)	12q13	Phosphate-activated glutaminase, a putative mitochondrial enzyme	1.54
D87009	Immunoglobulin λ variable 1-36 (*IGLV-36*)	22q11.2	Unknown	1.47

(continued)

tumors derive their growth advantage from more than a single aberrant molecular growth pathway leads to the combined molecular targeting approach." In our study, selected genes, for example, *NME2* (nonmetastatic cells 2), had an unclear function, although it has been reported that *NME2* exists in the *N-myc* and *c-myc* downstream pathway.[23] Recently, several epidemiologic findings that suggest sexual differences in lung adenocarcinoma, including the effectiveness of gefitinib in Asian female patients, have been presented. In addition, it has been reported that gefitinib was found to be effective in some patients who had no *EGFR* mutation.[24] Therefore, it is of great interest that any different carcinogenic mechanisms between